Thermodynamic properties of Nd-Fe alloys via emf measurements in LiCl-KCl-$NdCl_3$ electrolyte

Sanghyeok Im[a], Jarrod Gesualdi[a], Minkyu Kim[a,b], Peyman Asghari-Rad[a], Kelly Elizabeth Varnell[a], Hojong Kim[a*]

[a] Materials Science and Engineering, The Pennsylvania State University, University Park, PA 16802, United States

[b] Materials Science and Engineering, Inha University, Incheon 22212, Republic of Korea

Author Email Addresses:

svi5106@psu.edu, jqg5465@psu.edu, mxk6141@psu.edu, pza5214@psu.edu, kev5111@psu.edu, huk29@psu.edu

Corresponding Author:

[*]E-mail: huk29@psu.edu. Tel: 814-865-3117. Fax: 814-865-2917

KEYWORDS:

Neodymium-Iron alloys, emf measurements, open-circuit potentiometry, thermodynamic properties, rare-earth alloys

ABSTRACT

The thermodynamic properties of Nd-Fe alloys with varying mole fractions of Nd (x_{Nd} = 0.05–0.78) were investigated via electromotive force measurements in molten chloride at 773–1073 K. The Nd-Fe alloys were heat-treated at 923 K for 7 days to stabilize equilibrium phases, and the phase transition properties are confirmed by X-ray diffraction, electron microscopy, and differential scanning calorimetry. Employing less reactive Nd-Sn alloys (x_{Nd} = 0.10, L + $NdSn_3$) for a reference electrode, the measured emf values were consistent between alloy compositions, as shown by equivalent thermal trajectories in distinct two-phase regions of [Fe + Nd_2Fe_{17}], [Nd_2Fe_{17} + Nd_5Fe_{17}], [Nd_5Fe_{17} + Nd], [L + Nd_2Fe_{17}], and [L + Nd_5Fe_{17}]. The measured emf results were further validated using open-circuit potentiometry in which Nd was deposited onto an Fe electrode at 973 K, resulting in a difference of less than 18 mV for the identical two-phase alloy between the two methods.

1. INTRODUCTION

Neodymium metal is a key component of rare earth magnets (NdFeB), which are widely used in enabling green energy technologies (e.g., wind turbines, electric vehicles)[1,2] and currently produced via molten salt electrolysis (e.g., LiF-NdF_3-Nd_2O_3) at elevated temperature (~1373 K) in commercial scales.[3] In recent years, new electrochemical approaches have been investigated for the sustainable production of rare-earth alloys with improved efficiency at reduced emissions and recovery from secondary resources (e.g., NdFeB).[4,5]

Examples include (1) the recovery of rare-earth metals (Nd, Dy, Pr) from NdFeB scrap in molten salt electrolytes (LiCl-KCl and NaCl-KCl) at 873–1123 K,[6] (2) direct synthesis of Nd alloys (e.g., Nd-Fe and Nd-Ni) by electrodeposition of Nd onto a reactive cathode (Fe and Ni) in molten salt electrolytes (e.g., KCl-$NdCl_3$, LiF-CaF_2-NdF_3) at 1148 K,[7,8] and (3) direct electrolytic reduction of sintered (Nd, Fe)$_2O_3$ oxide into Nd-Fe alloys in $CaCl_2$-CaO at 1123 K.[9]

Despite recent efforts for direct electrochemical synthesis of Nd-Fe alloys and the popularity of NdFeB magnets in clean energy technologies, the thermodynamic and electrochemical properties of Nd-Fe alloys are not fully understood. Inconsistent results in the literature challenge the assumption of reliable control of electrode processes across published works. Thus, this work investigated the thermodynamic properties of binary Nd-Fe alloys by electromotive force (emf) measurements which are crucial in developing electrolytic processes for rare-earth alloys (e.g., Nd-Fe) and in materials simulation for reliable prediction of rare-earth alloys and compounds.

Broadly, thermodynamic properties of the Nd-Fe system were investigated via (1) emf measurements between pure Nd and Nd-Fe alloys using solid CaF_2 electrolyte by Hennemann et al.[10] and Gozzi et al.[11] and (2) open-circuit potentiometry following electrodeposition of Nd

onto an Fe electrode in molten salt electrolytes.[8,12,13] Henneman et al. conducted comprehensive emf measurements at a broad temperature range and reported a nearly constant emf value of ~0.08 V (vs. Nd) between 898–1073 K for two-phase [Fe + Nd_2Fe_{17}] compositions.[10] These results contrast with emf measurements of ~0.06 V between 998–1048 K using a CaF_2 electrolyte by Gozzi et al.,[11] ~0.32 V at 873 K by Konishi et al.,[13] and ~0.13 V at 1123 K by Kawaguchi and Nohira[8] via open-circuit potentiometry, illustrating inconsistencies in emf values.

To better understand the equilibrium potentials of Nd-Fe alloys, this work conducted emf measurements over a wide range of neodymium mole fractions (x_{Nd} = 0.05–0.78) and temperatures (773–1073 K) using a low-melting eutectic LiCl-KCl electrolyte ($T_{eutectic}$ = 626 K) with the addition of $NdCl_3$. These emf measurements were also compared with the open-circuit potentiometry at 973 K to validate the results. Compared to prior works, this work employed a Nd-Sn alloy (x_{Nd} = 0.10) as the reference electrode (RE) in LiCl-KCl-$NdCl_3$ electrolyte due to its exceptional stability with two [L + $NdSn_3$] phases; this stability was demonstrated in the authors' previous work in which an identical electrode showed a deviation of less than 3.5 mV over 45 days at 773–973 K.[14] In addition, the fabricated Nd-Fe alloys were characterized by differential scanning calorimetry (DSC) to determine phase transitions and by scanning electron microscopy (SEM) and X-ray diffraction (XRD) to ensure the presence of expected equilibrium phases.

To determine the emf of Nd-Fe alloys, the potentials of working electrode (WE) alloys with varying Nd alloy concentrations were measured relative to the RE (Nd-Sn alloy, x_{Nd} = 0.10), as described in the following electrochemical cell:

$$\underline{\text{Nd-Sn } (x_{Nd} = 0.10)} \mid \text{LiCl-KCl-NdCl}_3 \mid \text{Nd-Fe alloy} \quad (1)$$

The measured cell potential (E_I) is related to the ratio between the activity of Nd in Fe (a_{Nd}) and the activity of Nd in Sn (a^*_{Nd}) based on the Nernst equation as below:

$$E_{\mathrm{I}} = -\frac{RT}{3F}\ln\left(\frac{a_{\mathrm{Nd}}}{a^{*}_{\mathrm{Nd}}}\right) \quad (2)$$

where R is the universal gas constant, T is the Kelvin temperature, and F is the Faraday constant. Using the emf relation (E_{II}) between the RE and pure Nd at 724-1075 K as established in previous work [15],

$$E_{\mathrm{II}} = -\frac{RT}{3F}\ln(a^{*}_{\mathrm{Nd}}) = 0.590 + 1.52 \times 10^{-4}\, T \text{ [V]} \quad \text{vs.} \quad \text{Nd(s)} \quad (3)$$

, the cell potential (E_{I}) was converted to the emf (E_{eq}) of Nd-Fe alloys vs. Nd(s) at a given temperature. The determined emf was utilized to investigate thermodynamic properties such as the change in partial molar Gibbs energy ($\Delta\bar{G}_{\mathrm{Nd}}$) and chemical activity for Nd in Fe.

$$E_{\mathrm{eq}} = E_{\mathrm{I}} + E_{\mathrm{II}} = -\frac{RT}{3F}\ln(a_{\mathrm{Nd}}) = -\frac{\Delta\bar{G}_{\mathrm{Nd}}}{3F} \quad \text{vs.} \quad \text{Nd(s)} \quad (4)$$

2. METHODOLOGIES

2.1 Fabrication of Nd-Fe alloys and characterization

Nd-Fe alloys with specific compositions were prepared using a laboratory arc-melter (MAM-1, Edmund Bühler GmbH) from pure Nd (99.1%, Alfa Aesar) and Fe (99.98%, Alfa Aesar) metals under an inert Ar atmosphere. Phase transition temperatures of the Nd-Fe alloys (x_{Nd} = 0.05–0.78) were obtained using a thermal analyzer (Netzsch, STA 449 F3 Jupiter). Inert tungsten foil was placed between the sample alloy (20–50 mg) and the alumina crucible to block side reactions, and heat flow was measured at 473−1273 K with repeated heating/cooling at a rate of 5−20 K min^{-1} under flowing Ar (20 mL min^{-1}). The transition temperature for each alloy was determined by averaging the onset temperatures detected for all scan rates.

The microstructure of the Nd-Fe alloy was observed through a scanning electron microscope (SEM, FEI Quanta 200), and the composition of the arc-melted and heat-treated samples was analyzed using an energy dispersion spectrometer (EDS) to identify the phase

constituents. The Nd-Fe alloys were heat treated at 923 K for 7 days under an inert Ar atmosphere. The alloys were mounted in epoxy resin and surface-polished using SiC abrasive paper (2000 grit) with a constant flow of isopropyl alcohol for lubrication. The phase constituent of the heat-treated (equilibrated) Nd-Fe alloys was determined by X-ray diffraction (XRD, PANalytical Empyrean, Co Kα-radiation, 2-theta angles of 20−80°) analysis.

2.2 Electrochemical cell components

Electrolyte: The electrolyte was prepared by pre-melting a mixture of LiCl (Ultra dry, 99.9%, Alfa Aesar), KCl (Ultra dry, 99.95%, Alfa Aesar), and $NdCl_3$ (anhydrous, 99.5%, Alfa Aesar) with a composition of 57.9-41.6-0.5 mol% in a furnace (Mellen, CC-12) to ensure homogenization of the electrolyte. The salt mixture was placed in a quartz crucible within a stainless-steel vacuum chamber. The chamber was then sequentially heated to 373 K and held for 12 h under vacuum (~1 Pa) to dry, held at 543 K for 12 h for cell purging with Ar, and then held at 973 K for 3 h under flowing Ar (50 mL min^{-1}) to melt the salt. The pre-melted electrolyte was then crushed using a mortar and pestle.

Electrodes: The reference electrode (RE) was prepared using a Nd-Sn alloy (x_{Nd} = 0.10) and a BN crucible (8mm inner diameter, 2mm thickness, 35mm height) with two capillary holes (1 mm diameter) at a height of 7 mm. The Nd-Sn alloy for the RE was fabricated by arc-melting pure Nd (99.1%, Alfa Aesar) and Sn (99.9999%, Alfa Aesar) metals. 3 g of the arc-melted alloy was then placed in the BN crucible and remelted using an induction heater (IH15A-2T, Across International) in an Ar-atmosphere glovebox to insert the lead wire (tungsten, 99.95%, Thermo Shield, 1mm diameter).

In two-electrode cells (**Figure 1**a), the heat-treated Nd-Fe alloys served as the WEs for emf measurements. The Nd-Fe alloys were pulverized into granules using a mortar and pestle in the

glovebox and then pressed into a pellet (15 mm height, 8 mm diameter) by uniaxially pressing the powder at 20 MPa. The pellet was then placed into the BN crucible and a lead wire (molybdenum, 99.94%, Thermo Scientific Chemicals, 1mm diameter) was inserted into a vertical groove fabricated inside of the BN crucible to connect with the pellet.

In three-electrode cells (**Figure 1**b), the WE was prepared using tungsten (99.95%, Thermo Shield) and iron wires (99.9%, Alfa Aesar) with 45 cm length and 1mm diameter. The surface of the wires was polished with silicon carbide abrasive paper (1200 grit) in the glovebox to remove the oxide layer. The counter electrode (CE) was fabricated using a graphite rod (15 mm diameter, 35 mm length) tapped to accept a threaded stainless steel rod (3mm diameter, 45 cm length).

[Figure 1]

2.3 Electrochemical cell assembly and measurements

The electrochemical cells used in this work were prepared in an inert atmosphere glovebox filled with Ar. The pre-prepared electrodes were positioned in an alumina container (250mL, Advalue Technology), the electrical-leads were insulated by alumina tubes and closed with epoxy, and the electrolyte was poured into the alumina container to cover the electrodes (**Figure 1**). The test chamber was inserted into a stainless-steel vacuum chamber and assembled in the glove box. The prepared cells were transferred and loaded into a furnace and heated up to the operating temperature, through the same procedure described for electrolyte pre-melting.

A potentiostat/galvanostat (Autolab PGSTAT302N) was used for electrochemical data acquisition, and the operating temperature was recorded using a K-type thermocouple connected with a data collector (NI 9211, National Instruments).

3. RESULTS and DISCUSSION

To determine the thermodynamic properties of Nd-Fe alloys via emf measurements at 773–1073 K, the alloy electrodes must be in equilibrium during the measurements. However, the arc-melted Nd-Fe alloys exhibited non-equilibrium phases during solidification, necessitating heat treatment to stabilize the equilibrium phases. Thus, the phase behavior Nd-Fe alloys are first established via DSC to determine an appropriate temperature for stabilizing equilibrium phase constituents and to specify phase transitions during emf measurements.

3.1 Phase transition and constituents of Nd-Fe alloys

Phase transitions: DSC results for Nd-Fe alloys (x_{Nd} = 0.05–0.78) measured at 20 K min^{-1} heating rate are presented in **Figure 2**a, indicating three characteristic transitions (I-III). Each transition temperature (T_{trs}) was determined from the average of onset points for peak detected at four heating rates (5–20 K min^{-1}) from three different samples at each composition, and summarized in **Table 1**. These transition temperatures represent the eutectic reaction at 939 K [I: L ↔ Nd_5Fe_{17} + Nd], peritectic reaction at 1033 K [II: L + Nd_2Fe_{17} ↔ Nd_5Fe_{17}], and allotropic transition at 1209 K [III: Fe(ht) ↔ Fe(rt)], which are consistent with the prior experimental works [10,16–22] and overlaid on the binary Nd-Fe phase diagram (**Figure 2**b).[23]

[Figure 2] & [Table 1]

Phase constituents: The Nd-Fe alloys were prepared by arc-melting alloy compositions of x_{Nd} = 0.05, 0.15, and 0.50, representing distinct two-phase regions of [Fe + Nd_2Fe_{17}], [Nd_2Fe_{17} + Nd_5Fe_{17}], and [Nd_5Fe_{17} + Nd], respectively. However, the presence of non-equilibrium phases was evident for arc-melted alloys according to microstructural characterization by SEM-EDS (marked in red in **Figure 3**a), including the formation of unstable Nd-rich phases (x_{Nd} = 0.05, 0.15) and the absence of the equilibrium compound Nd_5Fe_{17} (x_{Nd} = 0.15, 0.50). Thus, these alloys were heat treated in the solid state, below the eutectic transition at 939 K (**Table 1)**, at 923 K for 7 days under

an inert argon atmosphere. After the heat treatment, the alloys exhibited two primary phases (**Figure 3**b), the compositions of the observed phase across the three alloys correspond to the expected equilibrium compounds of Fe, Nd_2Fe_{17} (x_{Nd} = 0.11), Nd_5Fe_{17} (x_{Nd} = 0.23), and Nd for each alloy. Two primary phase constituents of each alloy were also verified using XRD (**Figure 3**c), by comparing the diffraction pattern to the reported crystal structures in the Nd-Fe system,[24–29] summarized in **Table 2**. Overall, the heat treatment in the solid state was effective in stabilizing the equilibrium phases, required for emf measurements of Nd-Fe alloys.

[Figure 3] & [Table 2]

3.2 Emf of equilibrated Nd-Fe alloys

The cell potential of equilibrated Nd-Fe alloys (x_{Nd} = 0.05–0.78) was measured using a two electrode cell configuration (**Figure 1**a) in LiCl-KCl-$NdCl_3$ at 773–1073 K. The temperature was raised in increments of 25 K per 1.0 h during the heating cycle (**Figure 4**a). In general, the cell potential reached a steady value within 30 min at each temperature and the potential drift (dE_I/dt) in the steady state was minimal (< 0.18 mV min^{-1}). The notable exceptions include a near-eutectic composition of x_{Nd} = 0.78 which exhibited an unstable potential above 944 K due to the eutectic transition during the heating cycle. When the eutectic composition (x_{Nd} = 0.78) is held above the eutectic temperature at 977 K for 4 h in a separate experiment, a stable potential was obtained at 977–1073 K in the liquid state (**Figure 4**b).

[Figure 4]

The steady potential in the last 5 min was averaged as the emf (E_I) versus Nd-Sn (x_{Nd} = 0.10) at each temperature. E_I was then converted to E_{eq} relative to pure Nd based on the Eqs. (3–4). The emf of Nd-Fe alloys (E_{eq} vs. Nd) are plotted as a function of temperature for each composition (Figure **5**). The emf of x_{Nd} = 0.05 with two phases [Fe + Nd_2Fe_{17}] increased

monotonically with temperature with no indication of a phase transition. For x_{Nd} = 0.15, a peritectic transition at 1033 K delineates a phase transition from [Nd_2Fe_{17} + Nd_5Fe_{17}] to [L + Nd_2Fe_{17}]. At temperatures above 1033 K, the emf trajectory of x_{Nd} = 0.15 was comparable to that of x_{Nd} = 0.30 and 0.50 due to their identical phase behavior, [L + Nd_2Fe_{17}]. Emf values of x_{Nd} = 0.30 and 0.50 were close to each other (< 5 mV) and followed a similar emf trajectory at 773–1073 K (**Figure 4**a) due to their identical phase behavior across this temperature range.

[Figure 5]

For x_{Nd} = 0.78 near the eutectic composition, the emf for temperatures just below the eutectic temperature (939 K) were close to those of x_{Nd} = 0.30 and 0.50 as all three compositions exhibit similar phase behavior, [Nd_5Fe_{17} + Nd]. However, the emf values of x_{Nd} = 0.78 were consistently up to 21 mV lower than x_{Nd} = 0.30–0.50, possibly due to an increased fraction of the highly reactive Nd phase. Interestingly, the emf trajectory above the eutectic temperature (939 K) diverged from that of x_{Nd} = 0.30 and 0.50 due to its transition into single-phase liquid, distinct from two-phase [L + Nd_5Fe_{17}] behavior for x_{Nd} = 0.30 and 0.50.

After completing the measurements discussed, the Nd-Fe alloy electrodes were cooled from 1073 K to room temperature and characterized by SEM-EDS (**Figure 6**). The electrode at x_{Nd} = 0.05 maintained [Fe + Nd_2Fe_{17}] phases after the measurement since no phase transitions below 1073 K. However, non-equilibrium phases were observed in all other compositions (x_{Nd} = 0.15–0.78) due to the non-equilibrium cooling process from the liquid phase. The post-mortem characterization suggests that the emf measurements during cooling from the liquid phase will be less reliable owing to the formations of these non-equilibrium phases.

[Figure 6]

3.3 Thermodynamic properties of Nd-Fe alloys

The emf results of equilibrated Nd-Fe alloys were internally consistent, as can be seen from their decreasing value with increasing x_{Nd} at each temperature (**Figure 5**). Furthermore, a similar emf trajectory was observed between compositions in an identical two-phase region due to invariant activity, i.e., identical emf value, within these regions. Guided by characteristic transition temperatures from DSC (**Table 1**), the temperature-dependent emf (E_{eq} vs. T) was fitted for each distinct phase region using the following equation by least-squares regression :[30]

$$E_{eq} = A + BT + CT \ln T \qquad \text{[V] vs. Nd(s)} \tag{5}$$

The fitting parameters (A, B, C) and the standard error for the fitted line are shown in Table 3. Using this non-linear relation, the emf (E_{eq}), natural log of the activity ($\ln a_{\mathrm{Nd}}$), and the excess partial molar Gibbs energy ($\bar{G}^{E}_{\mathrm{Nd}}$) were calculated at 873 K and 973 K:

$$\bar{G}^{E}_{\mathrm{Nd}} = RT(\ln a_{\mathrm{Nd}} - \ln x_{\mathrm{Nd}}) = RT \ln \gamma_{\mathrm{Nd}} \tag{6}$$

where γ_{Nd} is the activity coefficient of Nd (**Table 4**). At 973 K, the E_{eq} of Nd-Fe is described as a function of x_{Nd}, demonstrating constant emf value at each two-phase region as well as the decrease in emf as Nd composition increases (**Figure 7**).

[Table 3] & [Table 4]

[Figure 7]

3.4 Emf measurements by transient techniques at 973 K

Using the Fe and inert W WEs in the three-electrode cell (**Figure 1**b), cyclic voltammetry (CV) and the transient technique of open-circuit potentiometry were employed in efforts to detect characteristic potentials relevant to phase behavior at 973 K. In CV measurements (**Figure 8**a), a

high current response was observed for Fe compared to the inert W electrodes by the alloying reaction between Nd and Fe beyond pure Nd deposition. However, no clear characteristic potential was observed related to the specific Nd-Fe alloy formation.

[Figure 8]

In contrast, the open-circuit potential measurements following constant current electrolysis at –50mA cm^{-2} for Nd deposition resulted in five characteristic potential plateaus, one for W and four for Fe electrodes (**Figure 8**b). For the inert W WE after Nd deposition, a potential plateau was observed near 0.0 V vs Nd(s), marked as (i) in **Figure 8**b, followed by rapid rise in potential due to the dissolution of pure Nd metal. For the Fe electrode, four characteristic potential plateaus (ii–v) were evident during the open-circuit potentiometry, suggesting the presence of four two-phase regions at 973 K. The potential at each plateau was determined from a steady value or inflection point for rapid transitions (iii–iv). According to the assessed phase diagram (**Figure 2**b), each potential represents two-phase behavior of [L + Nd] at 0.007 V, [L + Nd_5Fe_{17}] at 0.108 V, [Nd_5Fe_{17} + Nd_2Fe_{17}] at 0.181 V, and [Nd_2Fe_{17} + Fe] at 0.282 V, respectively. These plateau potentials at 973 K are in close agreement with the emf measurements of equilibrated alloys with a difference of less than 18 mV (**Figure 7**).

3.5 Comparison to prior works

Emf measurements of Nd-Fe alloys were performed by a number of researchers [8,10–13] based on (1) the equilibrated Nd-Fe alloys similar to the approach in section 3.2 and (2) open-circuit potentiometry of Fe electrode following electrodeposition (Li and Nd), similar to the approach in section 3.4. Hennemann et al.[10] and Gozzi et al.[11] employed a solid CaF_2 electrolyte and pure Nd RE for emf measurements of equilibrated Nd-Fe alloys, and reported the emf values of [Fe + Nd_2Fe_{17}] and [Nd_2Nd_{17} + Nd_5Fe_{17}] phases, marked in blue and red in **Figure**

9, respectively. Compared to this work, their emf values were substantially lower and remained nearly constant across the phase transitions at 939 K (eutectic) and 1033 K (peritectic). Such low emf values are thought to originate from the pure Nd RE with high reactivity which may react with the solid electrolyte and result in unreliable emf measurements. A similar issue was observed with a pure Nd RE as reported in an emf study for Nd-based alloys (e.g., Nd-Bi and Nd-Sn) in a solid CaF_2-NdF_3 electrolyte by Lichtenstein et al..[15] In their work, an irreversible decrease in emf values was noticeable after 20 h of emf measurement between 760–1035 K using pure Nd as the RE while the use of less-reactive Nd alloy (e.g., Nd-Sn) REs improved the reliability of emf measurements and extended the cell lifetime (> 50 h).

[Figure 9]

In contrast, Konish et al.[13], Kawaguchi and Nohira[8], and Yang et al.[12] reported the emf of Nd-Fe alloys based on the potential plateaus observed during open-circuit potentiometry following electrodeposition of Nd onto an Fe electrode in electrolytes of LiCl-$CaCl_2$-$NdCl_3$ (873 K), LiF-CaF_2-NdF_3 (1123 K), and LiF-NdF_3 (1221 K), respectively. When the prior emf values for [Fe + Nd_2Fe_{17}] phase behavior are compared at different temperatures (solid blue in **Figure 9**), the results do not exhibit a proper thermal trend (E_{eq} vs. T) and deviate from the results in this work. The inconsistency of these results may originate from the use of a transient open-circuit potentiometry technique where the detection of potential plateaus and assignment of relevant phase behavior are highly uncertain in the absence of reliable reference potential for Nd(III)/Nd and further complicated by co-deposition of Li and Nd in the preceding electrodeposition step.

4. CONCLUSIONS

Reliable emf measurements of Nd-Fe alloys were achieved by equilibrating the phase constituents of Nd-Fe alloys (x_{Nd} = 0.05–0.78) and utilizing a stable two-phase Nd-Sn alloy (x_{Nd} =

0.10) reference electrode in the LiCl-KCl-$NdCl_3$ (57.9-41.6-0.5 mol%) electrolyte at 773–1073 K. The measured emf values of Nd-Fe alloys in distinct two-phase regions were consistent between alloy compositions and were corroborated by thermal analysis and electrode characterization by XRD and SEM-EDS. In addition, the emf results agreed with the potential plateaus observed during the open-circuit potentiometry following electrodeposition of Nd onto Fe electrode at 973 K, suggesting the utility of this transient technique for estimating the thermodynamic properties and investigating the electrolytic formation of Nd-Fe alloys. Temperature-dependent emf values were employed to estimate thermodynamic properties of Nd in the Fe, including activity and excess partial molar Gibbs energy. This work suggests that reliable electrochemical property measurements of Nd alloys necessitate a stable reference electrode in place of reactive pure Nd. The reliable data and approach established in this work will provide a solid foundation in studying the thermodynamic properties of complex rare-earth alloys (e.g., Nd-Fe-B).

ACKNOWLEDGEMENTS

This work was supported by the U.S. National Science Foundation (NSF) with Grant No. CBET-1844170 and the MOTIE (Ministry of Trade, Industry, and Energy) in South Korea, under the Fostering Global Talents for Innovative Growth Program (P0017303) supervised by the Korea Institute for Advancement of Technology (KIAT).

REFERENCES

[1] U.S Department of Energy, Critical materials strategy, 2011.

[2] E.E. Union, Study on the review of the list of critical raw materials, 2017. https://doi.org/10.2873/876644.

[3] R. Akolkar, Perspective—Is Sustainable Electrowinning of Neodymium Metal Achievable?, J. Electrochem. Soc. (2022). https://doi.org/10.1149/1945-7111/ac6075.

[4] X. Xi, M. Feng, L. Zhang, Z. Nie, Applications of molten salt and progress of molten salt electrolysis in secondary metal resource recovery, Int. J. Miner. Metall. Mater. 27 (2020) 1599–1617. https://doi.org/10.1007/s12613-020-2175-0.

[5] W. Xiao, D. Wang, The electrochemical reduction processes of solid compounds in high temperature molten salts, Chem. Soc. Rev. 43 (2014) 3215–3228. https://doi.org/10.1039/C3CS60327J.

[6] A.M. Martinez, O. Kjos, E. Skybakmoen, A. Solheim, G.M. Haarberg, Extraction of Rare Earth Metals from Nd-based Scrap by Electrolysis from Molten Salts, ECS Trans. 50 (2013) 453. https://doi.org/10.1149/05011.0453ecst.

[7] S. Kobayashi, T. Nohira, K. Kobayashi, K. Yasuda, R. Hagiwara, T. Oishi, H. Konishi, Electrochemical Formation of Dy-Ni Alloys in Molten LiF-CaF_2-DyF_3, J. Electrochem. Soc. 159 (2012) E193–E197. https://doi.org/10.1149/2.053212jes.

[8] K. Kawaguchi, T. Nohira, Electrochemical Formation of Nd-Fe Alloys in Molten LiF-CaF_2-NdF_3, J. Electrochem. Soc. 168 (2021) 082503. https://doi.org/10.1149/1945-7111/ac180e.

[9] P.K. Tripathy, K. Mondal, A.R. Khanolkar, One-step manufacturing process for neodymium-iron (magnet-grade) master alloy, Mater. Sci. Energy Technol. 4 (2021) 249–255. https://doi.org/https://doi.org/10.1016/j.mset.2021.07.001.

[10] K. Hennemann, H.L. Lukas, H.-J. Schaller, Constitution and Thermodynamics of Fe-Nd Alloys, ZEITSCHRIFT FUR Met. 84 (1993) 668–674.

[11] D. Gozzi, M. Iervolino, A. Latini, Thermodynamics of Fe-rich intermetallics along the rare earth series, J. Chem. Eng. Data. 52 (2007) 2350–2358. https://doi.org/10.1021/je7003353.

[12] Y. Yang, R. Zhao, Z. Zhao, Electrochemical behaviors of neodymium ions on a solid iron electrode in molten lithium fluoride and reaction kinetics of forming Nd_2Fe_{17} intermetallic compound, Sep. Purif. Technol. 257 (2021) 117882. https://doi.org/10.1016/j.seppur.2020.117882.

[13] H. Konishi, H. Hua, H. Ono, Y. Koizumi, T. Oishi, T. Nohira, Electrochemical Formation of Dy-Fe and Nd-Fe Alloys in Molten $CaCl_2$-LiCl Systems, ECS Trans. 86 (2018) 321–328. https://doi.org/10.1149/08614.0321ecst.

[14] S. Im, N.D. Smith, S.C. Baldivieso, H. Kim, Electrochemical Cell Design for Emf Measurements of Liquid Nd-Bi Alloys via Coulombic Titration in LiCl-KCl-$NdCl_3$ Electrolyte, in: T. Ouchi, G. Azimi, K. Forsberg, H. Kim, S. Alam, N.R. Neelameggham,

A.A. Baba, H. Peng (Eds.), Rare Met. Technol. 2022, Springer International Publishing, Cham, 2022: pp. 317–324.

[15] T. Lichtenstein, S. Im, C.T. Yu, H. Kim, Thermodynamic properties of rare-earth alloys by electrochemical emf measurements, J. Mater. Res. (2021) 1–9. https://doi.org/10.1557/jmr.2020.218.

[16] Che Guangcan, Liang Jingkui, Wang Xuanzhang, PHASE DIAGRAM OF Nd-Fe-B TERNARY SYSTEM., Sci. Sin. Ser. A. Math. Phys. Astron. Tech. Sci. 29 (1986) 1172–1185. https://doi.org/10.1360/ya1986-29-11-1172.

[17] M.A. Van Ende, I.H. Jung, Critical thermodynamic evaluation and optimization of the Fe-B, Fe-Nd, B-Nd and Nd-Fe-B systems, J. Alloys Compd. 548 (2013) 133–154. https://doi.org/10.1016/j.jallcom.2012.08.127.

[18] B. Konar, J. Kim, I.H. Jung, Critical Systematic Evaluation and Thermodynamic Optimization of the Fe-RE System: RE = La, Ce, Pr, Nd and Sm, J. Phase Equilibria Diffus. 37 (2016) 438–458. https://doi.org/10.1007/s11669-016-0473-z.

[19] T.L. Chen, J. Wang, M.H. Rong, G.H. Rao, H.Y. Zhou, Experimental investigation and thermodynamic assessment of the Fe-Pr and Fe-Nd binary systems, Calphad Comput. Coupling Phase Diagrams Thermochem. 55 (2016) 270–280. https://doi.org/10.1016/j.calphad.2016.10.004.

[20] G. Schneider, E.-T. Henig, B. Grieb, G. Knoch, Phase Equilibria in Fe-Nd-B and Related Systems and Microstructure of Sintered Fe-Nd-B Magnets, Concert. Eur. Action Magnets. (1989) 335–357. https://doi.org/10.1007/978-94-009-1135-2_29.

[21] F. Faudot, M. Harmelin, J. Bigot, The Iron-Neodymium Phase Diagram, Scr. Metall. 23 (1989) 795–798. https://doi.org/10.1016/0036-9748(89)90533-4.

[22] F.J.G. Landgraf, G.S. Schneider, V. Villas-Boas, F.P. Missell, Solidification and solid state transformations in FeNd: A revised phase diagram, J. Less-Common Met. 163 (1990) 209–218. https://doi.org/10.1016/0022-5088(90)90101-O.

[23] Thermo-Calc Software TC Binary Solutions version 1.1 database, (2016).

[24] S. Ohba, Y. Saito, Y. Noda, A measurement of charge asphericity in iron metal, Acta Crystallogr. Sect. A. 38 (1982) 725–729. https://doi.org/10.1107/S0567739482001454.

[25] A.T. Gorton, G. Bitsianes, T.L. Joseph, Thermal expansion coefficients for iron and its oxides from X-ray diffraction measurements at elevated temperatures, Trans. Metall. Soc. AIME. 233 (1965) 1519.

[26] T. Kajitani, Y. Morii, S. Funahashi, T. Iriyama, K. Kobayashi, H. Kato, Y. Nakagawa, K. Hiraya, High-resolution neutron powder diffraction study on nitrogenated Nd_2Fe_{17}, J. Appl. Phys. 73 (1993) 6032–6034. https://doi.org/10.1063/1.353460.

[27] J.M. Moreau, L. Paccard, J.P. Nozieres, F.P. Missell, G. Schneider, V. Villas-Boas, A new phase in the NdFe system: Crystal structure of Nd_5Fe_{17}, J. Less-Common Met. 163 (1990) 245–251. https://doi.org/10.1016/0022-5088(90)90590-G.

[28] F.H. Spedding, A.H. Daane, K.W. Herrmann, The crystal structures and lattice parameters of high-purity scandium, yttrium and the rare earth metals, Acta Crystallogr. 9 (1956) 559–563. https://doi.org/10.1107/S0365110X5600156X.

[29] F.H. Spedding, J.J. Hanak, A.H. Daane, High Temperature allotropy and thermal expansion of the rare-earth metals, J. Less-Common Met. 3 (1961). https://doi.org/10.1016/0022-5088(61)90003-0.

[30] A. Petric, A.D. Pelton, M.L. Saboungi, Thermodynamic properties of liquid K-Bi alloys by electromotive force measurements, J. Phys. F Met. Phys. 18 (1988) 1473–1489. https://doi.org/10.1088/0305-4608/18/7/015.

FIGURES

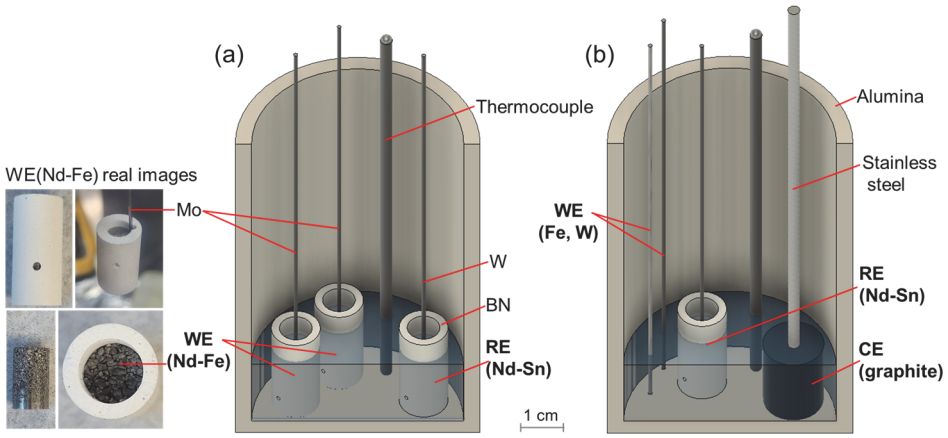

Figure 1. (a) Two-electrode cell for emf measurements of Nd-Fe alloys (x_{Nd} = 0.05–0.78) using Nd-Sn alloys (x_{Nd} = 0.10) as the RE and (b) three-electrode cell using W and Fe as the WE and graphite as the CE in LiCl-KCl-$NdCl_3$ (57.9-41.6-0.5 mol%) electrolyte.

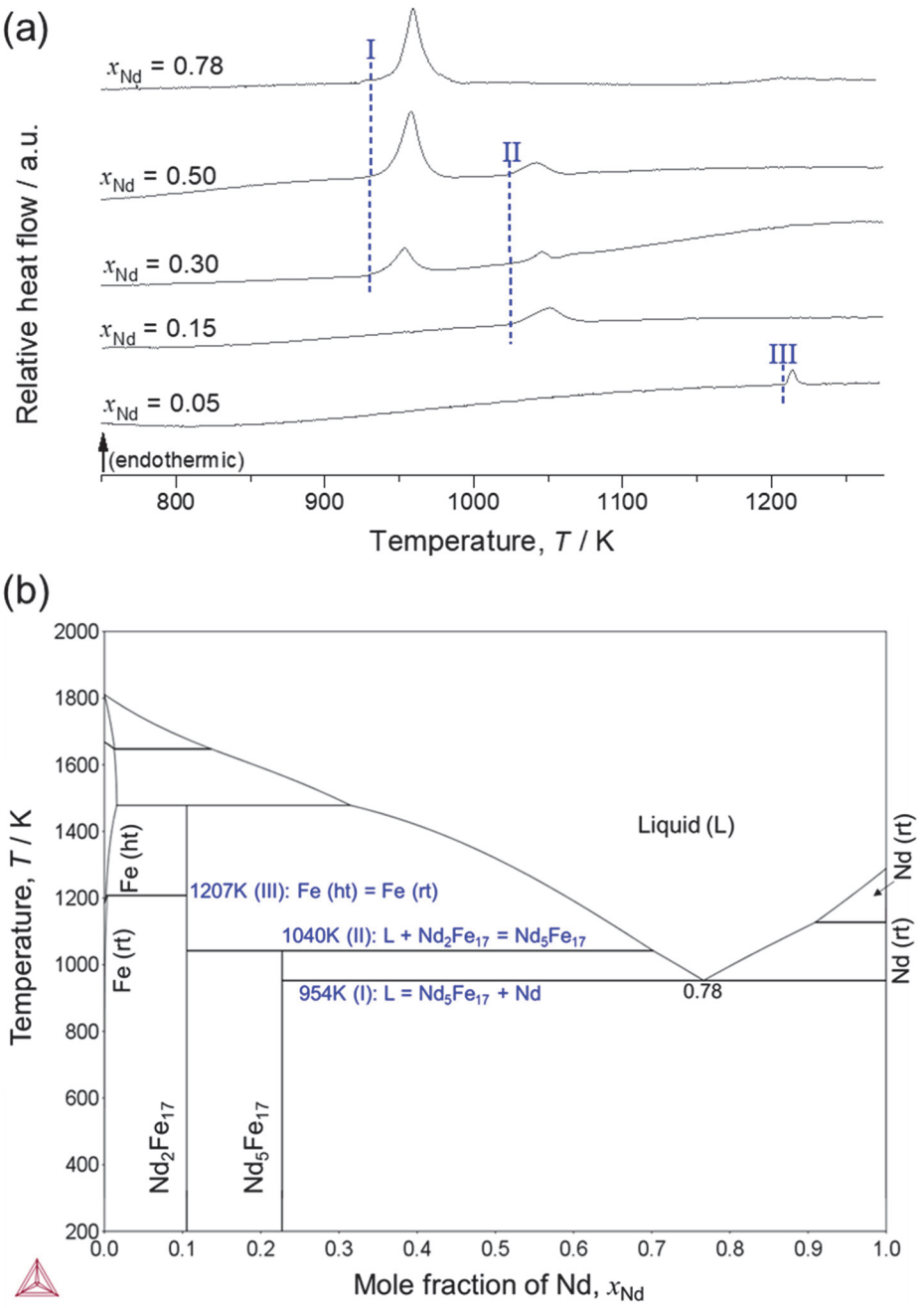

Figure 2. (a) DSC measurements of the Nd-Fe alloys (x_{Nd} = 0.05–0.78) at 20 K min^{-1} heating rate and (b) binary Nd-Fe phase diagram by Thermocalc®,[23] where roman numerals (I–III) represent detected characteristic phase transitions by DSC.

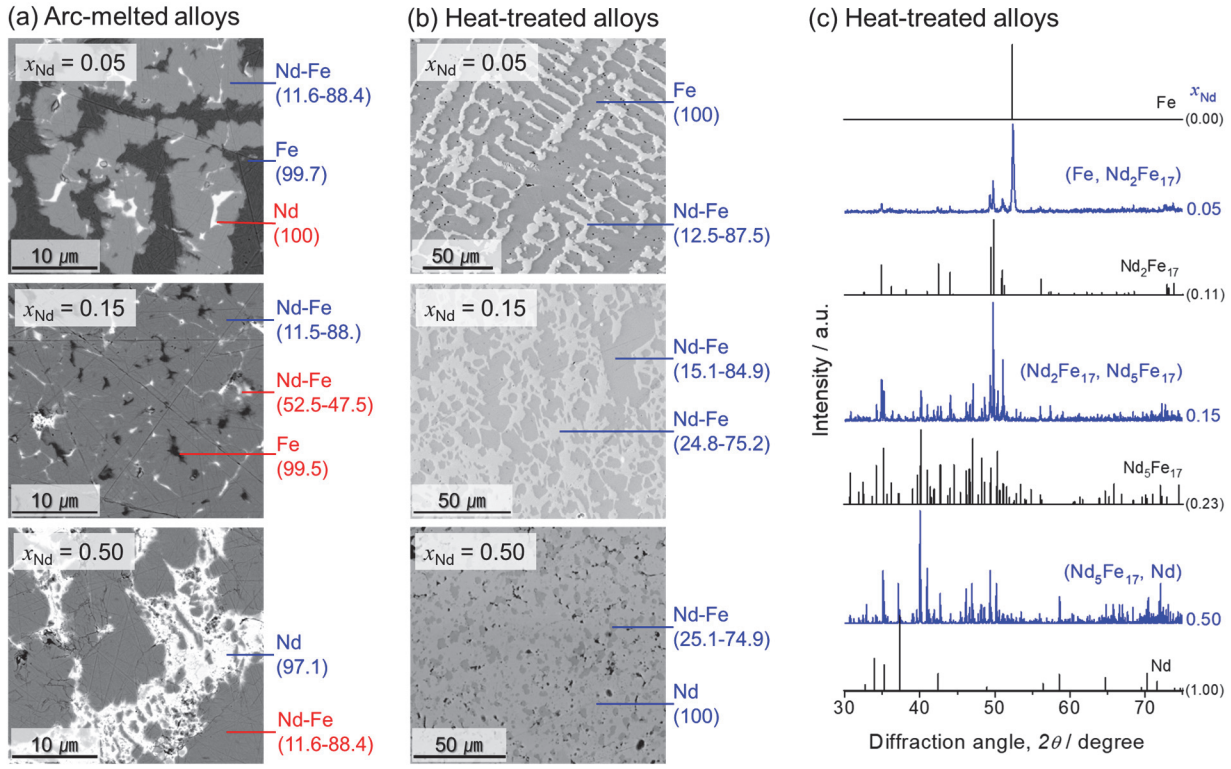

Figure 3. SEM images of Nd-Fe alloys at x_{Nd} = 0.05, 0.15, 0.50: (a) arc-melted samples, (b) heat-treated samples at 923 K for 7 days, with approximate phase composition (at%) in the parenthesis by EDS, and (c) XRD patterns of the heat-treated Nd-Fe alloys compared to the reported patterns of Fe, Nd_2Fe_{17}, Nd_5Fe_{17}, and Nd. [24–29]

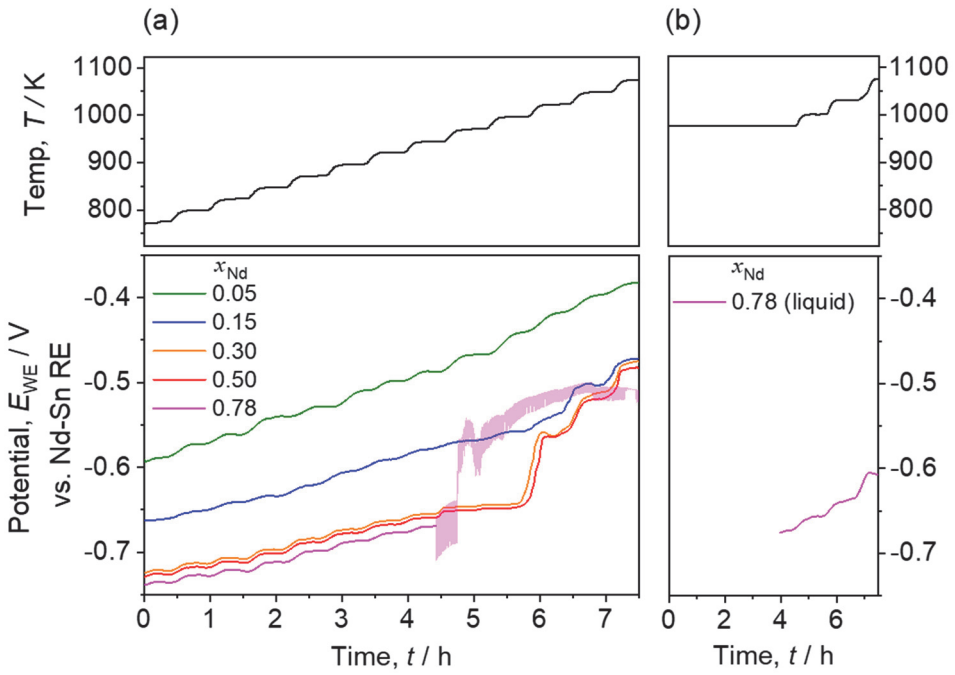

Figure 4. The cell potential of (a) equilibrated Nd-Fe alloys (x_{Nd} = 0.05–0.78) versus Nd-Sn (x_{Nd} = 0.10) during the heating at 773–1073 K and (b) liquid Nd-Fe alloy (x_{Nd} = 0.78) at 977–1073 K after melting at 977 K for 4 h above the electrolyte.

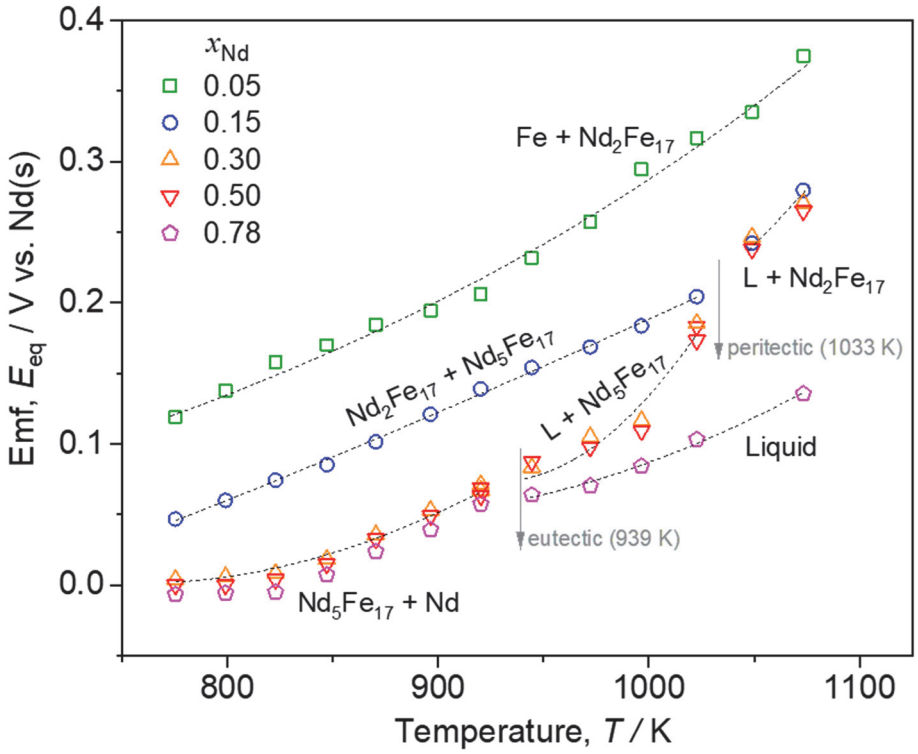

Figure 5. Emf (E_{eq} vs. Nd) of the Nd-Fe alloys (x_{Nd} = 0.05–0.78) as a function of temperature (773–1073 K), where the dotted lines are non-linear fits to the data for each phase region.

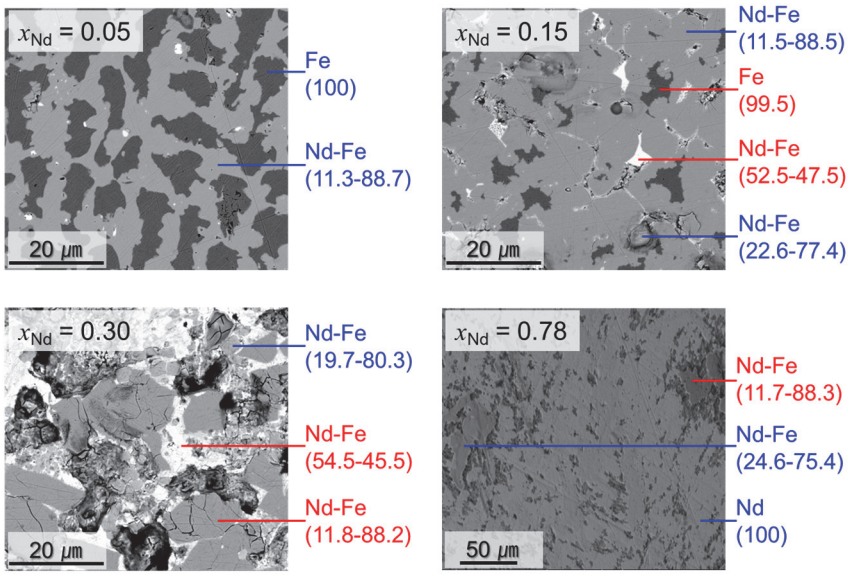

Figure 6. SEM images of the Nd-Fe alloys (x_{Nd} = 0.05–0.78) after emf measurements at 1073 K with phase composition by EDS for estimating each phase constituent.

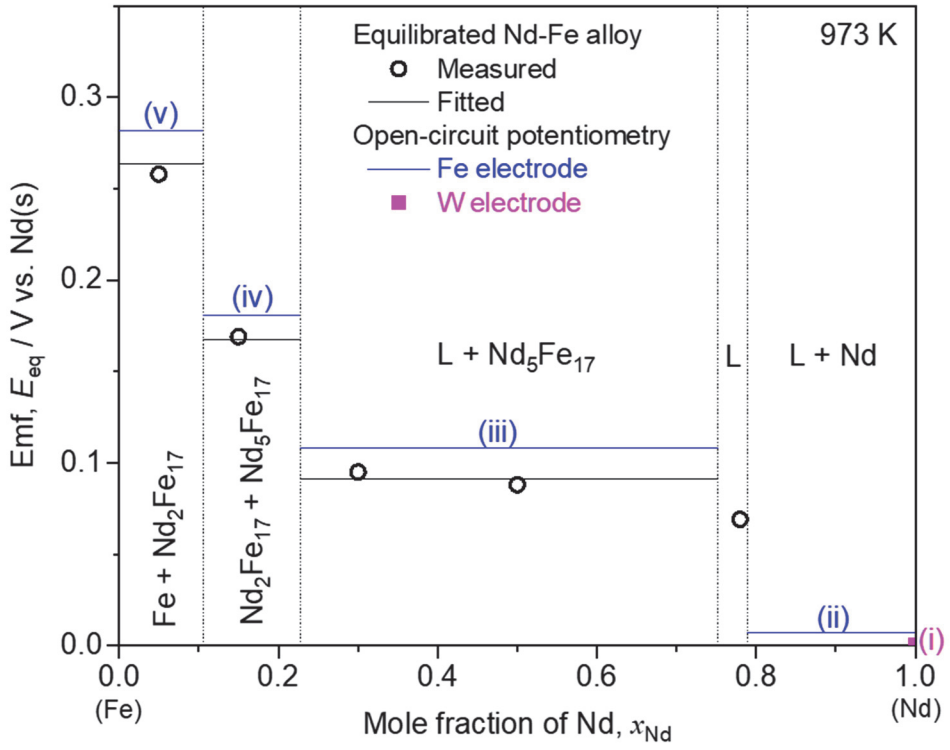

Figure 7. Emf (E_{eq}) of Nd-Fe alloys as a function of x_{Nd}, compared to characteristic potentials detected in open-circuit potentiometry at 973 K.

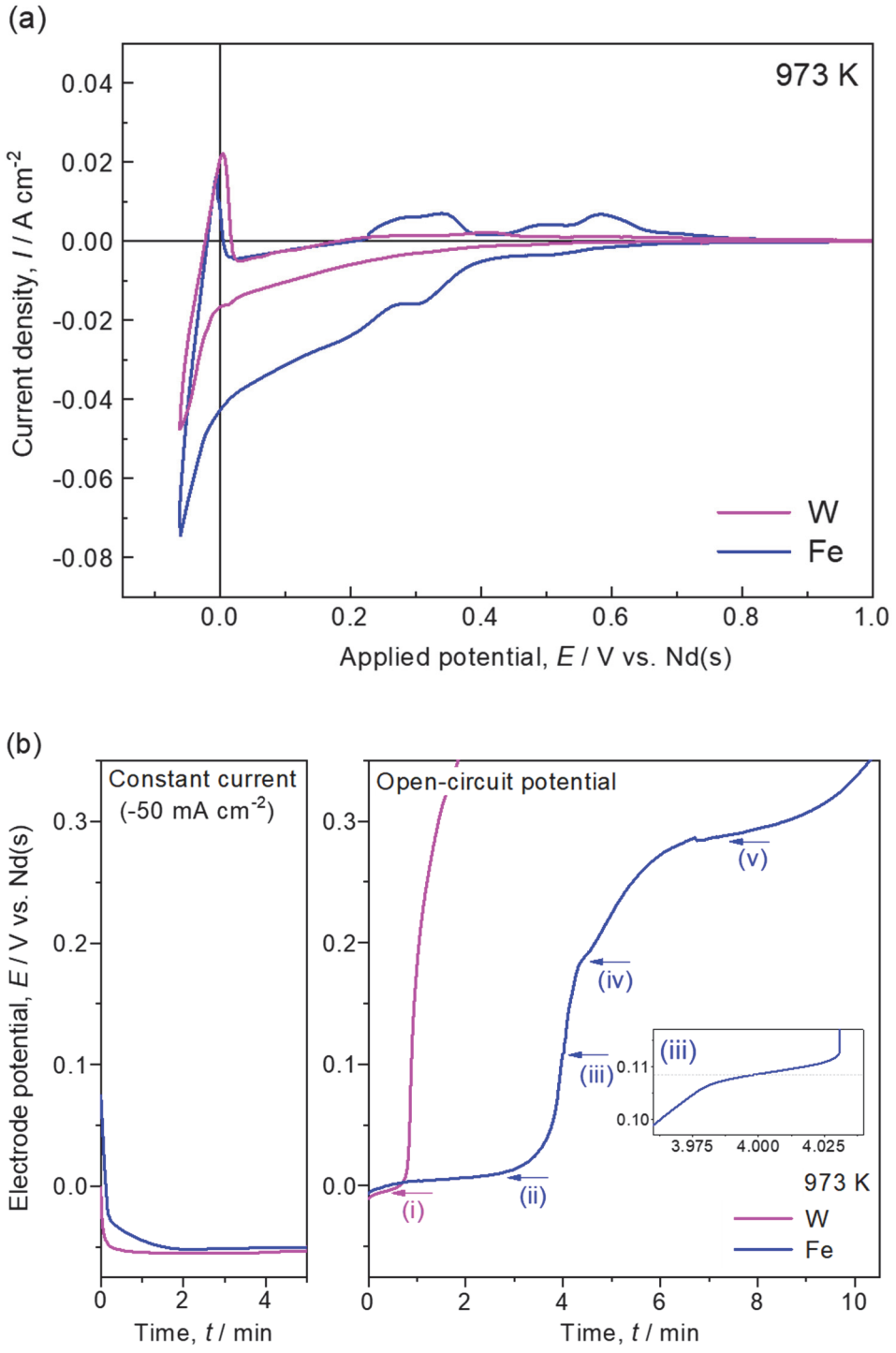

Figure 8. (a) Cyclic voltammograms (*E* vs. Nd) at 25 mV s^{-1} and (b) constant current electrolysis for Nd deposition at −50 mA cm^{-2} for 5 min (left), followed by open-circuit potentiometry (right), using iron and tungsten WEs in molten LiCl-KCl-$NdCl_3$ at 973 K.

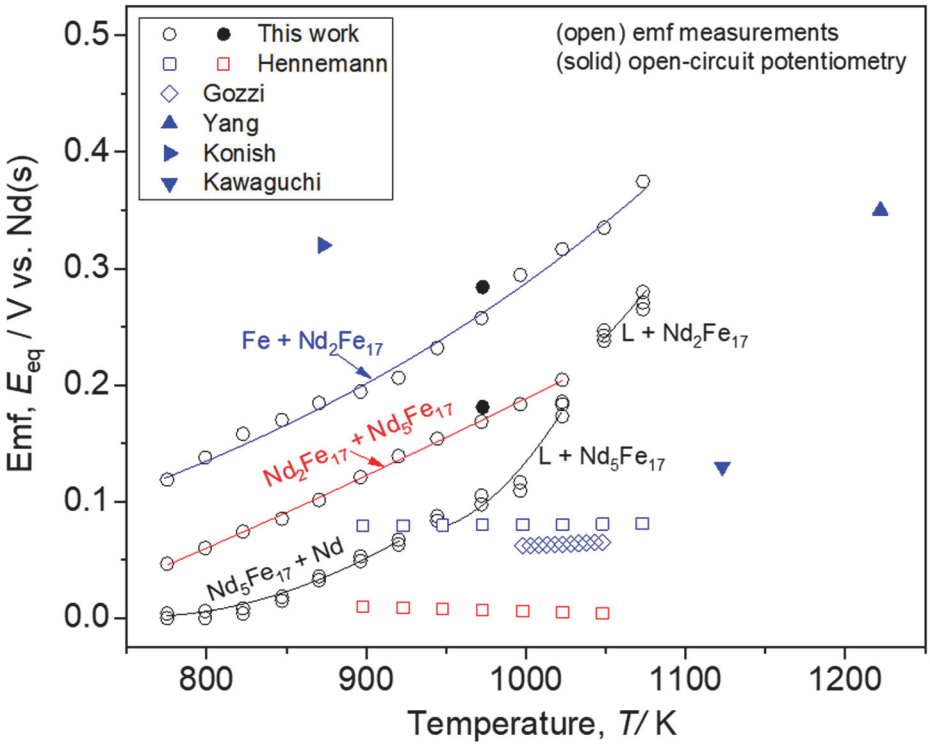

Figure 9. Emf of Nd-Fe alloys in two-phase regions as a function of temperature in this work compared to the results from prior works indicated in blue for [Fe + Nd_2Fe_{17}] and in red for [Nd_2Fe_{17} + Nd_5Fe_{17}], respectively [8,10–13].

TABLES

Table 1. Three characteristic transition temperatures (T_{trs}) and reactions of Nd-Fe alloys from DSC measurements compared to the prior experimental works.

Transition (Type)	Reaction	T_{trs} (K)	
		This work	Previous works
I (Eutectic)	$L \leftrightarrow Nd_5Fe_{17} + Nd$	939 (±3.6)	920–958 [10,16–22]
II (Peritectic)	$L + Nd_2Fe_{17} \leftrightarrow Nd_5Fe_{17}$	1033 (±4.5)	1044–1071 [10,17–19,22]
III (Allotropic)	Fe (ht) ↔ Fe (rt)	1209 (±1.5)	1183–1208 [10,16–19]

Table 2. Phase constituents of Nd-Fe alloys from arc melting and after heat treatment at 923 K for 7 days by SEM-EDS and XRD. Non-equilibrium phases in arc-melted alloys are underlined.

x_{Nd}	Detected phase constituents	
	arc-melted alloy	heat-treated alloy
0.05	Fe, Nd_2Fe_{17}, <u>Nd</u>	Fe, Nd_2Fe_{17}
0.15	<u>Fe</u>, Nd_2Fe_{17}, <u>Nd</u>	Nd_2Fe_{17}, Nd_5Fe_{17}
0.50	<u>Nd_2Fe_{17}</u>, Nd	Nd_5Fe_{17}, Nd

Table 3. Non-linear fits of the temperature dependence of emf data for x_{Nd} = 0.05–0.78 in Figure 5 using $E_{eq} = A + BT + CT \ln T$ ([V] vs. Nd) for each phase region. The standard errors in the parentheses represent the 95% confidence interval of the fit.

x_{Nd}	Phase behavior	T (K)	A	B [$\times 10^{-3}$]	C [$\times 10^{-3}$]	adj-R^2
0.05	Fe + Nd_2Fe_{17}	775–1073	1.7235 (±0.44)	-18.389 (±3.77)	2.4549 (±0.48)	0.992
0.15	Nd_2Fe_{17} + Nd_5Fe_{17}	775–1023	-0.1496 (±0.22)	-2.0101 (±0.19)	0.3395 (±0.02)	0.998
0.15–0.50	L + Nd_2Fe_{17}	1047–1073	3.3073 (±0.02)	-33.648 (±0.19)	4.4168 (±0.02)	1.000
0.30–0.50	Nd_5Fe_{17} +Nd	775–921	3.9140 (±0.79)	-38.689 (±7.24)	5.0600 (±0.93)	0.996
0.30–0.50	L + Nd_5Fe_{17}	944–1023	21.172 (±4.92)	-178.07 (±39.5)	22.731 (±5.01)	0.977
0.78	Liquid	944–1073	3.1364 (±1.59)	-27.890 (±12.5)	3.6001 (±1.59)	0.988

Table 4. Measured emf of Nd-Fe alloys, natural log activity ($\ln a_{Nd}$), and excess partial molar Gibbs energy ($\bar{G}^E_{Nd}$) of Nd at 873 K and 973 K.

x_{Nd}	E_{eq} (V) vs. Nd		$\ln a_{Nd}$		$\bar{G}^E_{Nd}$ (kJ mol^{-1})	
	873 K	973 K	873 K	973 K	873 K	973 K
0.5	0.184	0.258	-7.38	-9.22	-31.7	-50.3
0.15	0.101	0.169	-4.06	-6.04	-15.6	-33.5
0.30	0.039	0.095	-1.55	-3.40	-2.5	-17.8
0.50	0.034	0.088	-1.34	-3.14	-4.7	-19.8
0.78	0.024	0.069	-0.95	-2.48	-5.1	-18.1